DOI: 10.61782/fa.2023.0324

forum acusticum 2023

ACTIVE ACOUSTIC SU-SCHRIEFFER-HEEGER-LIKE SYSTEM

Mathieu Padlewski[1*] **Maxime Volery**[1] **Romain Fleury**[2]
Hervé Lissek[1] **Xinxin Guo**[1]
[1] Acoustic Group - Signal Processing Laboratory LTS2, EPFL, Lausanne, Switzerland
[2] Laboratory of Wave Engineering LWE, EPFL, Lausanne, Switzerland

ABSTRACT

An acoustic dimer composed of two electronically controlled electro-acoustic resonators is presented in view of exploring one dimensional topological phenomena. Active control allows for real-time manipulation of the metamaterial's properties, including its mechanical mass, resistance, compliance and internal coupling. The latter enables active tuning of topological phase transition in the effective acoustic Su–Schrieffer–Heeger system. The electronic control scheme used for simultaneous impedance synthesis and dimerisation of the unit cell is presented. Band structures derived from finite element simulations and the experimental data consistently demonstrate control of band-folding Bragg gap size by the user-tunable dimerisation parameter.

Keywords: *Active control, topology, SSH*

1. INTRODUCTION

This study presents an actively tuneable acitve metamaterial capable of exhibiting prescribed topological features similar to those found in the Su–Schrieffer–Heeger system [1] - a one dimensional chain of coupled dimers that can host topological modes owing to its two coupling-dependant regimes. We demonstrate an actively tuneable dimer composed of two electronically-controlled Active Electro-acoustic Resonators (AERs) [2]. We present the active control scheme used to tune dimerisation of the unit cell and experimentally measure the bulk meta-crystal dispersion. Fidelity of the measurement is supported by finite element simulations.

*__Corresponding author__: *mathieu.padlewski@epfl.ch.*

2. TAILORING THE DISPERSION THROUGH ACTIVE CONTROL

Suppose a crystal unit cell composed of a duct segment loaded with two identical and equally spaced AERs that are fixed in place as shown in Fig 1a.

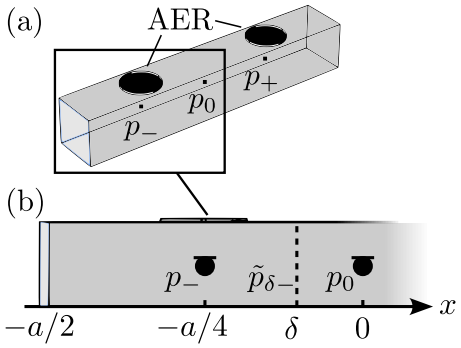

Figure 1. Active dispersion shaping using two identical and equally spaced AERs. Black dots in the unit cell are control microphones.

A periodic array of these cells with coupling would form a SSH-like chain along the x axis. In order to achieve active impedance control, the experimental unit cell is equipped with microphones placed in front and in between of the lined AERs as shown in Fig. 1b. The system is tuned via an active feedback control scheme which is split in two parts - each of which aims at altering the gaps present in the dispersion of the coupled resonator meta-structure, namely a band folding *Bragg gap* and a *locally resonant gap*, highlighted in Fig. 2.

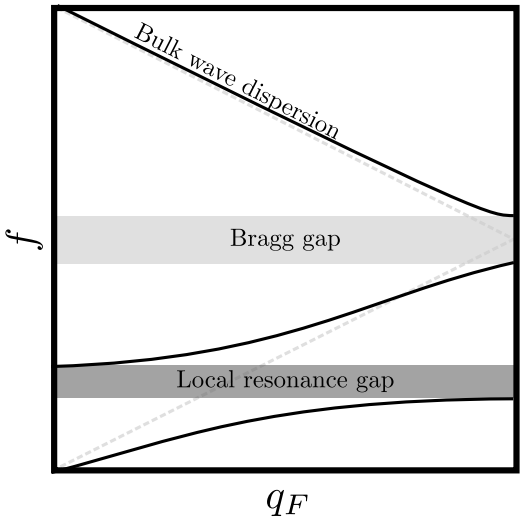

Figure 2. Typical dispersion of a lossless coupled resonator system. There are with two gaps: a Bragg gap (light grey) and a locally resonant gap (dark grey).

2.1 Shaping the locally resonant gap

The band-folding *locally resonant gap* results from the coupling of a continuum of propagating waves and a local resonance which can be described by a polariton-like dispersion [3] - albeit folded for a doubled unit cell. Its position and size can be shaped at the experimenter's discretion by altering the AER's resonance frequency and quality factor [4–6]. The desired mechanical impedance ζ_{st} is specified by control parameters $\mu_M, \mu_R, \mu_C \in \mathbb{R}_+^*$:

$$\zeta_{st}(s) = \mu_M M_{ms} \cdot s + \mu_R R_{ms} + \mu_C/(C_{mc} \cdot s) \quad (1)$$

Where:

- $s = j\omega$: Laplace variable
- M_{ms}: diaphragm mass (kg)
- R_{ms}: mechanical resistance (kg.s^{-1})
- C_{mc}: diaphragm + cabinet compliance (m.N^{-1})

ζ_{st} synthesis is achieved by multiplying a transfer function $\Phi(\zeta_{st})$ to the real-time front pressure resulting in the current required to drive the AERs [2].

2.2 Shaping the Bragg gap

The band-folding *Bragg gap* opens when dimerisation is introduced in the crystal [1]. Here we show that a gap forms when the coupling is enhanced via active control. Fig. 3 shows the proposed block diagram of the control scheme. Knowing the operating wavenumber k in the waveguide, the pressure $\tilde{p}_{\delta\pm}$ between an AER and the centre microphones can be estimated using the function:

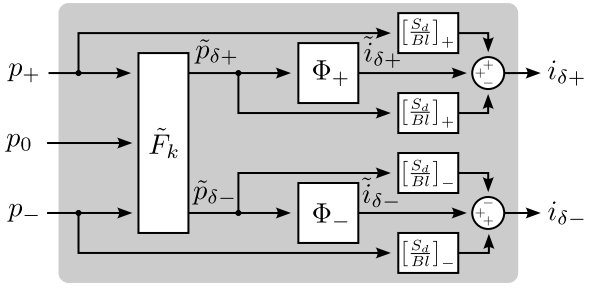

Figure 3. Block diagram of the proposed control scheme wired to the experimental unit cell. From left to right, the acoustic pressures in front of and in between the AERs (- $p_\pm$ and p_0 respectively) are used as inputs of the $\tilde{F}_k$ function which serves to achieve the δ shift. The impedance is synthesized with the desired mechanical parameters specified by the transfer functions $\Phi_\pm$. The output currents $i_{\delta\pm}$ are carried out to the respective AERs in the unit cell.

$$\tilde{F}_k(p_\pm, p_0) \coloneqq \frac{p_\pm \cdot \sin(\pm k(a/4 - \delta)) + p_0 \cdot \sin(\pm k\delta)}{\sin(\pm ka/4)} \quad (2)$$

where δ is the dimerisation parameter.

The virtual control current required to synthesize a target impedance Z_{st} is:

$$\tilde{i}_{\delta\pm} = \tilde{p}_{\delta\pm} \cdot \Phi_\pm \quad (3)$$

where $\Phi_\pm$ is the aforementioned transfer function. Notice that Φ appears twice in the control scheme block diagram as the AERs mechanical parameters are synthesized separately.

Finally, the control current $i_{\delta\pm}$ used to drive the AERs are:

$$i_{\delta\pm} = (p_\pm - \tilde{p}_{\delta\pm}) \cdot \left[\frac{S_d}{Bl}\right]_\pm + \tilde{i}_{\delta\pm} \quad (4)$$

3. DIRECT BAND STRUCTURE MEASUREMENT

The experimental meta-crystal bulk band structure or dispersion is obtained by direct measurement of the unit

cell transfer matrix M_{cell} by means of a Kundt tube and four pressure microphones as shown in Fig. 4 (according to the ASTM E2611-09 standard [7]).

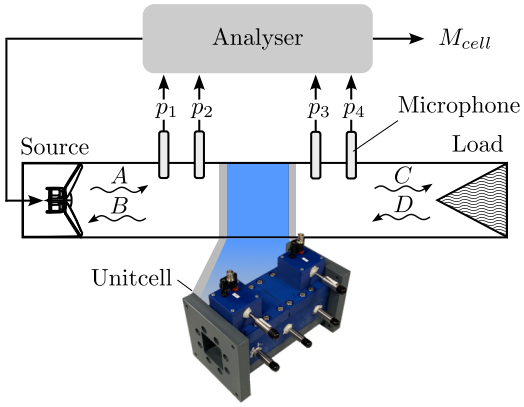

Figure 4. Characterisation of the transfer matrix of a sample using a loaded Kundt duct and four pressure microphones. Spatial separation of the microphones on both sides of the sample allows for the determination of the forward (a,c) and backward (b,d) complex field amplitudes.

The transfer matrix M_{cell} is directly obtained from the scattering matrix which links the outgoing complex field amplitudes (b, c) to the ingoing (a, d):

$$M_{cell} = \begin{pmatrix} S_{21} - \frac{S_{22}S_{11}}{S_{12}} & \frac{S_{22}}{S_{12}} \\ \frac{-S_{11}}{S_{12}} & \frac{1}{S_{12}} \end{pmatrix} \tag{5}$$

where, for a symmetric and reciprocal system:

$$\begin{aligned} S_{11} = S_{22} &= \frac{ABe^{jka} - CDe^{-jka}}{A^2e^{jka} - D^2e^{-jka}} \\ S_{12} = S_{21} &= \frac{AC - BD}{A^2e^{jka} - D^2e^{-jka}} \end{aligned} \tag{6}$$

Finally the experimental band structure is obtained by applying the Floquet-Bloch theorem the the latter yielding:

$$q_F(k) = \arccos\left(\frac{1}{2}Tr(M_{cell}(k))\right)/a \tag{7}$$

where q_F is the Floquet-Bloch wave number.

4. RESULTS AND DISCUSSION

One active SSH-like unit-cell was successfully designed, 3D-printed and assembled. The experimental AERs are off-the-shelf Vistaton FRWS 5 8Ω drivers. Characterization of the mechanical parameters of the latter was achieved by direct measurement of the impedance following methods described by E. Rivet [2] using quarter-inch PCB microphones and a single-point Polytec laser vibrometer for simultaneous pressure and velocity measurement respectively. The mass, resistance and compliance were characterised and actively tuned as summarised in the Table 1. The goal was first to decrease the resonance frequency and second, to increase the quality factor of the resonators. The former effectively increases the locally resonant gap and Bragg gap frequency separation and the latter decreases system losses (see Fig. 2).

Table 1. Impedance synthesis. The passive mechanical parameters of the AER are multiplided by the respective tuning parameters $\mu_{M,R,C}$ to obtain the desired synthesised mechanical parameters.

	Mass	Resistance	Compliance
Passive	5.29 g	0.297 kg/s	175 μm/N
$\mu_{M,R,C}$	0.5	0.09	0.42
Synthesized	2.65 g	0.0267 kg/s	73.5 μm/N

Active control is carried out by a commercial Speedgoat machine equipped with the IO334 module. Experimentally measured dispersion curves are plotted in Fig. 5b for various dimerization parameter values δ. Moreover, COMSOL Multiphysics finite element simulations were performed enabling design optimization and experimental validation. Using the "Pressure Acoustics, Frequency Domain" module, each lined speaker is modelled using the experimentally obtained lumped parameters. Electronic control feedback delay ($\approx 50\mu s$) is taken into account to reliably capture the physics. The scattering matrix elements S11 and S12 - consequently M_{cell} - are obtained using ports at the extremities of the simulated unit-cell yielding dispersion curves shown in Fig. 5a.

Remarkable consistency can be noticed throughout both the ideal finite element simulations and the experimental results reflecting the efficacy of the proposed active control scheme. In particular, the Bragg gaps open

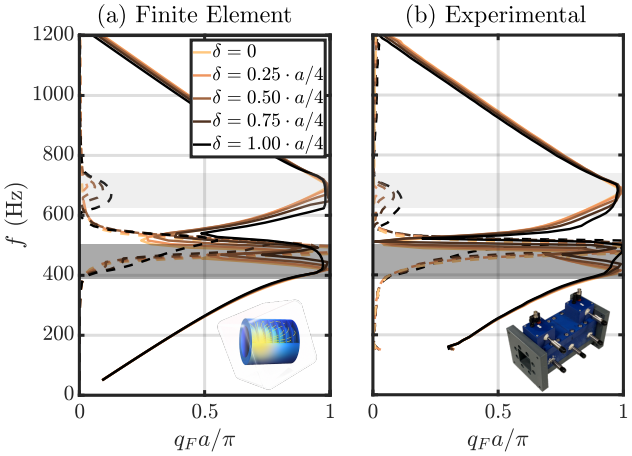

Figure 5. Active control on the band gap size. The dispersion diagrams of the acoustic SSH-like for five values of the dimerisation parameter δ derived from the finite element simulation (a) and measured experimental data (b). Solid lines and dashed lines represent the real and imaginary parts of the Bloch-Floquet wave number q_F respectively. The largest Bragg gap is indicated by the light grey bar and the locally resonant gap by the dark grey bar (c.f Fig. 2).

as a function of the user-defined electronic dimerisation parameter δ.

5. CONCLUSION

An active dimer composed of two electronically controlled AERs was presented. We demonstrated a current control scheme that enables shaping of both the locally resonant and the Bragg gaps. One active unit-cell was built and characterized by measuring its transfer matrix and subsequently deriving the dispersion curve by applying Bloch theorem. The experimental meta-crystal dispersion curves closely matched those obtained from finite element simulations. Most notably, we showed that the locally resonant gap and the Bragg gap could be easily shaped via speaker impedance synthesis and dimerisation parameter tuning δ respectively. Owing to the wide tunability and reconfigurability, the presented active unit cell opens up a new path to seek out novel physical phenomena such as those involving time-modulated interaction, time reversal symmetry breaking or non-linearity.

6. ACKNOWLEDGMENTS

This research is supported by the Swiss National Science Foundation (SNSF) under grant No. 200020_200498.

7. REFERENCES

[1] W. P. Su, J. R. Schrieffer, and A. J. Heeger, "Solitons in polyacetylene," *Physical Review Letters*, vol. 42, pp. 1698–1701, jun 1979.

[2] E. Rivet, S. Karkar, and H. Lissek, "Broadband Low-Frequency Electroacoustic Absorbers Through Hybrid Sensor-/Shunt-Based Impedance Control," *IEEE Transactions on Control Systems Technology*, vol. 25, no. 1, pp. 10. 63–72, 2017.

[3] S. Yves, R. Fleury, F. Lemoult, M. Fink, and G. Lerosey, "Topological acoustic polaritons: Robust sound manipulation at the subwavelength scale," *New Journal of Physics*, vol. 19, no. 7, 2017.

[4] E. Rivet, S. Karkar, and H. Lissek, "On the optimisation of multi-degree-of-freedom acoustic impedances of low-frequency electroacoustic absorbers for room modal equalisation," *Acta Acustica united with Acustica*, vol. 103, pp. 1025–1036, nov 2017.

[5] H. Lissek, E. Rivet, T. Laurence, and R. Fleury, "Toward wideband steerable acoustic metasurfaces with arrays of active electroacoustic resonators," *Journal of Applied Physics*, vol. 123, no. 9, 2018.

[6] X. Guo, H. Lissek, and R. Fleury, "Improving Sound Absorption Through Nonlinear Active Electroacoustic Resonators," *Physical Review Applied*, vol. 13, no. 1, p. 1, 2020.

[7] ASTM.E2611-09, "Standard Test Method for Measurement of Normal Incidence Sound Transmission of Acoustical Materials Based on the Transfer Matrix Method 1," *American Society for Testing and Materials*, vol. i, 2011.